



## Effect of increasing thickness on tensile-strained germanium grown on InGaAs buffer layers

M. de Kersauson, M. Prost, A. Ghrib, M. El Kurdi, S. Sauvage et al.

Citation: *J. Appl. Phys.* **113**, 183508 (2013); doi: 10.1063/1.4804266

View online: <http://dx.doi.org/10.1063/1.4804266>

View Table of Contents: <http://jap.aip.org/resource/1/JAPIAU/v113/i18>

Published by the American Institute of Physics.

---

### Additional information on J. Appl. Phys.

Journal Homepage: <http://jap.aip.org/>

Journal Information: [http://jap.aip.org/about/about\\_the\\_journal](http://jap.aip.org/about/about_the_journal)

Top downloads: [http://jap.aip.org/features/most\\_downloaded](http://jap.aip.org/features/most_downloaded)

Information for Authors: <http://jap.aip.org/authors>

## ADVERTISEMENT

**AIP Advances**

Now Indexed in  
Thomson Reuters  
Databases

Explore AIP's open access journal:

- Rapid publication
- Article-level metrics
- Post-publication rating and commenting

# Effect of increasing thickness on tensile-strained germanium grown on InGaAs buffer layers

M. de Kersauson,<sup>1,a)</sup> M. Prost,<sup>1,2</sup> A. Ghrib,<sup>1</sup> M. El Kurdi,<sup>1</sup> S. Sauvage,<sup>1</sup> G. Beaudoin,<sup>3</sup> L. Largeau,<sup>3</sup> O. Mauguin,<sup>3</sup> R. Jakomin,<sup>3</sup> I. Sagnes,<sup>3</sup> G. Ndong,<sup>4</sup> M. Chaigneau,<sup>4</sup> R. Ossikovski,<sup>4</sup> and P. Boucaud<sup>1,b)</sup>

<sup>1</sup>Institut d'Electronique Fondamentale, CNRS-Univ. Paris-Sud 11, Bâtiment 220, F-91405 Orsay, France

<sup>2</sup>STMicroelectronics, 850 rue Jean Monnet, 38920 Crolles, France

<sup>3</sup>Laboratoire de Photonique et de Nanostructures, CNRS-UPR 20, Route de Nozay, F-91460 Marcoussis, France

<sup>4</sup>Laboratoire de Physique des Interfaces et des Couches Minces, CNRS-Ecole polytechnique, F-91128 Palaiseau, France

(Received 31 October 2012; accepted 23 April 2013; published online 9 May 2013)

We have investigated the optical properties of tensile-strained germanium grown on InGaAs buffer layers as a function of film thickness and buffer layer composition. We study the dependence of the photoluminescence as a function of the strain amplitude and degree of relaxation which are also monitored by X-ray diffraction and Raman spectroscopy. We show that 0.75% biaxially strained germanium can be obtained up to a thickness of 150 nm, a value sufficiently high to allow confinement of the spontaneous emission in a guiding structure. For large thicknesses ( $>200$  nm) and large indium content in the buffer layer, a partial relaxation of the film is observed characterized by a large in-plane anisotropy of the germanium lattice. In this case, a difference of strain magnitude deduced either by microphotoluminescence spectra or by X-ray or Raman measurements is reported. We explain this difference by the sensitivity of microphotoluminescence to the local properties of the material. This study provides guidelines in order to achieve high optical quality and high biaxial tensile strain in Ge films with thicknesses compatible with optical waveguiding. © 2013 AIP Publishing LLC. [<http://dx.doi.org/10.1063/1.4804266>]

## INTRODUCTION

The lack of an efficient light emitter compatible with standard silicon processing has been hindering the development of silicon photonics for decades. Various methods have been investigated so far to integrate an optical source on silicon like III–V bonding,<sup>1,2</sup> GeSn alloying,<sup>3</sup> stimulated Raman emission,<sup>4</sup> or the use SiGe self-assembled nanostructures.<sup>5</sup> Pure germanium has only recently become a potential candidate. Despite the compatibility of germanium with silicon processes, germanium is an indirect band gap semiconductor material and the use of an indirect band structure has long been considered as inappropriate to achieve lasing. However, the recent demonstration of a germanium-based laser operating at room temperature<sup>6</sup> indicates that the difficulties due to the indirect band gap can be overcome. Two key features can explain this change of paradigm: the use of tensile strain and heavy *n*-type doping.

Applying a tensile strain shrinks the 136 meV energy difference between the minimum of the indirect conduction *L* valley and direct conduction  $\Gamma$  valley.<sup>7</sup> It also lifts the degeneracy between the heavy and light hole bands, decreasing the carrier density needed for population inversion. With a 1.9%–2% tensile strain, the energy difference between *L* and  $\Gamma$  valleys vanishes thus leading to an equivalent direct band gap material. Achieving such high strain is

technologically challenging, and even more challenging if we consider thick layers. Such large strain is nonetheless not mandatory to obtain optical gain with tensile-strained germanium. Even smaller values can be useful to reduce the carrier density needed to achieve optical transparency.<sup>8</sup> Another ingredient to achieve positive optical gain is the use of heavy *n*-type doping. In the latter case, the low energy states of the indirect *L* valley are filled by the introduction of dopants in the germanium. This increases the quasi-Fermi energy in the conduction band and leads to a more efficient population of zone-center  $\Gamma$  valley. Consequently, the strain needed to obtain a positive gain for a given injected carrier density is reduced.<sup>9,10</sup> As an example, for *n*-doped germanium with  $2 \times 10^{19} \text{ cm}^{-3}$  doping, only  $1 \times 10^{19} \text{ cm}^{-3}$  photo-induced carrier density is required to achieve optical transparency when a 0.6% biaxial strain is present.

The recent germanium laser demonstration relied on the thermal dilatation coefficient mismatch between Ge and Si to apply some strain.<sup>6</sup> This approach allows the growth of thick layers of strained germanium, but is limited to a maximum of 0.25% tensile strain.<sup>11</sup> Increasing this strain would allow one to reach a higher gain, consequently allowing the fabrication of structures with smaller footprints and smaller threshold power. Other approaches without strain limitations are thus being investigated. Among them, the stressor layer deposition has recently made some progress, by reaching biaxial strain as high as 1.13% in germanium membranes<sup>12</sup> or by the demonstration of optical gain in Ge photonic wires.<sup>13</sup>

<sup>a)</sup>Electronic mail: malo.de-kersauson@u-psud.fr

<sup>b)</sup>URL: <http://pages.ief.u-psud.fr/QDgroup>

Another approach is the use of III–V buffer layers as templates for the growth of tensile-strained germanium.<sup>15</sup> Though it is not a direct growth on silicon, it can be seen as an intermediate step before bonding just as SiGe buffer layers are used to grow tensile-strained silicon that can later be bonded on a silicon substrate through an intermediate oxide layer. The growth on lattice-mismatched  $\text{In}_{1-x}\text{Ga}_x\text{As}$  allows one to tailor the strain by varying the indium content in the alloy. Although it is not bound by the 0.25% strain limit, this type of heteroepitaxy is limited by the plastic relaxation occurring beyond a critical thickness. This critical thickness decreases when the strain increases. Very high strain, up to 2.33%, can be achieved with thin layers of a few nanometers.<sup>16,17</sup> But with the goal of achieving a laser, a minimum thickness of the order of  $\lambda/2n$ , i.e., typically hundreds of nanometers, is needed to ensure a waveguiding effect in the germanium layer. The strain amplitude is thus limited by the requirement to reach this minimum guiding thickness without plastic relaxation. In this letter, we present the results of our study of germanium grown on InGaAs buffer layers and discuss the optical quality of the layers and the suitability of this approach to grow tensile-strained germanium.

## SAMPLE GROWTH

Our study covers five different nominal indium concentrations for the InGaAs buffer layer from 4.8% to 15%. For each concentration, different samples were grown with a thickness ranging from 25 nm up to 300 nm. The samples were grown by metal-organic vapor phase epitaxy (MOVPE) using  $\text{H}_2$  as carrier gas. Both III–V and Ge are deposited in the same growth chamber. Trimethyl-indium, trimethyl-gallium, and arsine are used at low pressure (70 Torr) as In, Ga, and As precursors. The InGaAs buffer layer is 1  $\mu\text{m}$  thick, to ensure the relaxation of the buffer. X-ray diffraction measurements showed that the relaxation amount for the buffer was not complete, ranging from 80% to 95% depending on the indium percentage. To account for this partial relaxation, we use in the following discussion an effective indium content which represents the indium composition needed to have the same lattice parameter with a fully relaxed buffer. Thus, the study covers effective indium contents from 4.5% to 13%. For Ge growth, we use an isobutyl-germane source compatible with the III–V gas exhaust system. During this last step, an  $\text{AsH}_3$  flow is maintained in order to prevent As desorption from the buffer layer, and to obtain *in situ* doping of *n*-type around  $10^{19} \text{ cm}^{-3}$  in the germanium layer.

## X-RAY DIFFRACTION MEASUREMENTS

X-ray diffraction measurements were made on some samples using XPertPro Panalytical and Smartlab Rigaku diffractometers in triple axis geometry. We have reported in a previous publication results for thin Ge layers of 25 and 50 nm and indium composition varying between 4.8% and 9.8%.<sup>18</sup> A limited number of samples were investigated due to the weakness of the signal coming from such thin layers. In the latter case, X-ray diffraction measurements showed a maximum tensile strain of 0.5%, a full strain transfer from InGaAs to Ge, a good crystalline structure, and a purely

tetragonal deformation of Ge. The situation is significantly different for X-ray diffraction patterns of thick Ge layers deposited on buffer layers with a rich indium composition. We illustrate this effect for a sample with a large germanium thickness (250 nm) and high indium content for the buffer layer, i.e., beyond the onset of plastic relaxation.

Fig. 1 shows X-ray reciprocal space mappings around (004) direction for a 250 nm thick germanium on an InGaAs buffer with a 13% effective indium content. Fig. 1(a) corresponds to the mapping along the 180° azimuthal direction while Fig. 1(b) corresponds to the mapping along the 90° azimuthal direction. From top to bottom, the spots correspond vertically to the signature of Ge, GaAs, and InGaAs layers. As expected, the GaAs diffraction spot is the most intense and the narrowest. The InGaAs has a higher lattice parameter than GaAs in the growth direction. It thus appears below gallium arsenide on the graph. The germanium spot appears above GaAs on the graph, meaning the *c* parameter is lower than its bulk value which should be quasi-identical to the GaAs lattice parameter at ambient temperature. This is coherent with a shortening of the *c* parameter because of in-plane tensile strain. The uniformity of the strain in the growth direction is confirmed by the absence of vertical extension in the germanium diffraction spot. The horizontal extension of the InGaAs and Ge spots indicates some misorientations between different crystalline planes. This corresponds to a mosaicity of the lattice both for InGaAs and Ge that is attributed to defects and plastic relaxation of the buffer layer. Fig. 1(a) taken with a 180° azimuthal direction shows that InGaAs and GaAs diffraction spots are vertically aligned. This is not the case in Fig. 1(b) taken along the 90° (or -90°) azimuthal direction. This misalignment of the order of 0.42° is significant and associated with a misorientation between the (004) planes of InGaAs and GaAs as a consequence of the plastic relaxation of the buffer. There is however no misorientation between Ge and InGaAs. The misorientation is only observed in two azimuthal directions (90° and -90°). This could be due to a larger density of dislocations in InGaAs along one direction as compared to the other. As a consequence of the misorientation between GaAs

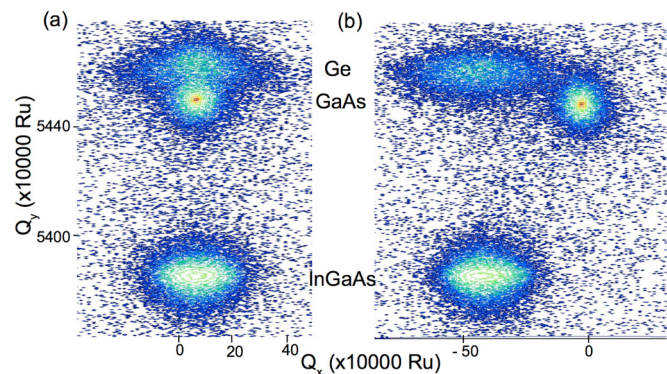


FIG. 1. High-resolution X-ray diffraction reciprocal space mapping around (004) reflection. The germanium film is 250 nm thick and was grown on an InGaAs buffer layer with an effective indium content of 13%. The diffraction spots correspond to Ge, GaAs, and InGaAs from top to bottom. (a) X-ray reciprocal space mapping around (004), in-plane azimuthal direction: 180°. (b) X-ray reciprocal mapping around (004), azimuthal direction 90°.

and InGaAs, equivalent to a miscut substrate, we observe a deviation from tetragonality for the germanium lattice, i.e., the lattice parameter along one in-plane direction is different from the lattice parameter along the perpendicular in-plane direction. In order to quantify this tetragonality deviation, X-ray reflection spectra were also measured along (115) and (-1-15) directions (not shown). The misorientation between InGaAs and GaAs is the same as the one measured for the (004) reflection. By combining these measurements, one can deduce the in-plane and out-of-plane lattice parameters. The out-of-plane lattice parameters are almost independent of the azimuthal directions (0.564054 nm along 0° and 180°, 0.564040 for -90° and 90°). The in-plane lattice parameter is however very dependent on the directions: 0.567998 nm for 0° and 180° azimuths, 0.566964 for -90°, 90° azimuths. As compared to the bulk Ge value found in the literature (0.56578 nm), the in-plane strain is thus 0.39% for 0°, 180° azimuthal directions and 0.21% for -90°, 90° azimuthal directions. The crystalline deformation is thus far from biaxial. If we deduce the strain from the germanium lattice parameter deduced from the measurement, the strain is 0.45% along 0°, 180° directions and 0.27% along -90°, 90° directions. The average lattice parameter values are shown in Table I for the 250 nm thick sample.  $a_0$  is calculated using the relations  $\varepsilon_{\perp} = -2(C_{12}/C_{11})\varepsilon_{\parallel}$ ,  $\varepsilon_{\perp} = [(a_{\perp} - a_0)/a_0]$ ,  $\varepsilon_{\parallel} = [(a_{\parallel} - a_0)/a_0]$  and  $2(C_{12}/C_{11}) = 0.698$  from which we deduce  $a_0 = 0.58893 a_{\perp} + 0.41107 a_{\parallel} = 0.56546$  nm.

The average biaxial strain for this sample is thus 0.3%-0.36% depending on the bulk germanium lattice value used to deduce the strain, much below the expected strain value if plastic relaxation did not occur (0.91%). It is important to notice that the calculated in-plane value results from an average over all in-plane directions and over a large surface area probed by the X-ray beam. The average strain measured by X-ray is thus not necessarily identical to the strain probed by the carriers involved in photoluminescence. This will be discussed later when we analyze the photoluminescence spectra.

One may wonder if this strain in-plane anisotropy ( $\varepsilon_{xx} \neq \varepsilon_{yy}$ ) has an impact on the band structure. It turns out that the effect is negligible as compared to a biaxial situation where  $\varepsilon_{xx}$  and  $\varepsilon_{yy}$  are chosen equal to the average of the measured  $\varepsilon_{xx}$  and  $\varepsilon_{yy}$  values. The effect of strain on the band structure is taken into account through the Bir-Pikus Hamiltonian.<sup>14</sup> In this Hamiltonian, there are off-diagonal matrix coefficients which are proportional to the difference between  $\varepsilon_{xx}$  and  $\varepsilon_{yy}$ . These terms couple the heavy hole, the light hole and the spin-orbit bands. If the strain is not biaxial, these terms are non zero. They are proportional to a deformation potential (eV range) times the strain difference and

TABLE I. Average lattice parameters for a 250 nm thick Ge sample grown on a 1 μm thick InGaAs buffer layer with a 13% effective indium content. All values are in nm.

	$a_{\perp}$	$a_{\parallel}$	$a_0$ calculated	$a_0$ from literature
InGaAs	0.57215	0.57056	0.57154	0.57148
Ge	0.564047	0.567481	0.56546	0.56578

couple bands that are independently split by the trace of the strain tensor. The energy correction is thus proportional to  $V^2/E$  where  $V$  is the coupling parameter (meV range) and  $E$  is the energy difference between the bands (30 meV range). The energy correction is thus very small and not significant. It only induces a sub-meV shift of the state energies. By performing a full calculation with or without these off-diagonal terms (i.e., without biaxial assumption and  $\varepsilon_{xx} = 0.45\%$ ,  $\varepsilon_{yy} = 0.27\%$  (off-diagonal elements non zero) or using an effective biaxial assumption  $\varepsilon_{xx} = \varepsilon_{yy}$  = average value of 0.36% (off-diagonal elements equal to zero)), the correction is around 500 μeV for the heavy hole and light hole bands. It can be neglected and has no effective impact on the band structure. Note that we have not considered the shear components. For the same arguments as explained above, the correction due to shear strain is also expected to be small. We can thus consider an effective biaxial strain for the photoluminescence and energy band structures. For the Raman measurements described below, the Raman shift measured in the normal backscattering geometry along the (001) direction depends on the sum of the diagonal elements  $\varepsilon_{xx}$  and  $\varepsilon_{yy}$  as can be seen from Eq. (2) in Ref. 19. The in-plane strain discussed below  $\varepsilon_{\parallel}$  is given by  $\varepsilon_{\parallel} = (\varepsilon_{xx} + \varepsilon_{yy})/2$ .

## RAMAN MEASUREMENTS

The strain state of the samples can also be investigated by Raman spectroscopy using a back-scattering geometry. We used a Labram HR800 Raman spectrometer (HORIBA Jobin Yvon) equipped with a confocal microscope (Olympus BX41) and an optical pump at 532 nm, corresponding to a penetration depth in germanium around 20 nm. Under the assumption of biaxial strain, one can deduce the strain magnitude from the spectral shift of the Ge-Ge phonon vibration mode around 300 cm<sup>-1</sup>. Fig. 2 shows an example of Raman spectra measured for samples of varying thicknesses grown on a buffer layer with an equivalent indium content of 7.8%. There is a clear red-shift of the Raman peak as compared to bulk germanium, indicating a tensile strain state for the germanium layer. One can observe that the shift is not as large for the 150 nm thick sample. It indicates that a partial relaxation has occurred for this sample. An important parameter to extract the strain amplitude is the link between the spectral shift in cm<sup>-1</sup> and the biaxial strain according to the relation  $\Delta\omega = -b\varepsilon_{\parallel}$ . The  $b$  parameter depends on the phononic and

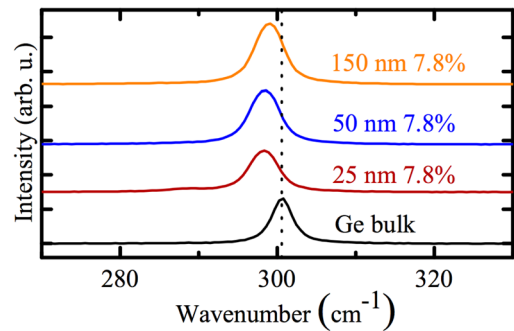


FIG. 2. Raman measurements showing the shift of the Ge-Ge phonon vibration. The thickness of the Ge layer and the indium composition of the buffer layer are indicated on the graph.

elastic constants of the studied material. Different values of the  $b$  parameter can be found in the literature for germanium. The standard value for bulk germanium is  $415\text{ cm}^{-1}$ .<sup>15</sup> Slightly different values have been deduced from the combined study by Raman and X-ray diffraction of silicon-germanium alloys,  $384\text{ cm}^{-1}$  in Ref. 20 as well as  $450\text{ cm}^{-1}$ <sup>21</sup> or  $460\text{ cm}^{-1}$ .<sup>22</sup> It is not excluded that this coefficient could depend on the thickness of the germanium layer. One has also to be very careful to avoid thermal effects when performing Raman measurements. In our case, a satisfying agreement is obtained between X-ray and Raman measurements either for coherently strained layers or partially relaxed buffer layers if we use a conversion coefficient of  $415\text{ cm}^{-1}$ . For a  $50\text{ nm}$  thick Ge layer grown on an InGaAs buffer layer with an equivalent indium content of 7.8%, the biaxial strain measured by X-ray diffraction is 0.5% and 0.48% by Raman. For the partially relaxed layer as shown in Fig. 1 (250 nm thick germanium on an InGaAs buffer with a 13% effective indium content), the average strain measured by X-ray is 0.3%–0.36% while the strain measured by Raman is 0.29%. The average values for strain measured by Raman or X-ray diffraction are thus equivalent and one can use either method to characterize the layers that are either coherently strained or plastically relaxed.

## PHOTOLUMINESCENCE MEASUREMENTS

The room temperature photoluminescence was excited at normal incidence by a 3 mW  $632.8\text{ nm}$  He-Ne laser in a microphotoluminescence set-up using the same objective for excitation and collection. The luminescence is dispersed in a spectrometer with a  $55\text{ cm}$  focal length and measured by an extended InGaAs photodetector array with a cut-off wavelength at  $2.1\text{ }\mu\text{m}$ . Figures 3(a)–3(d) show the room

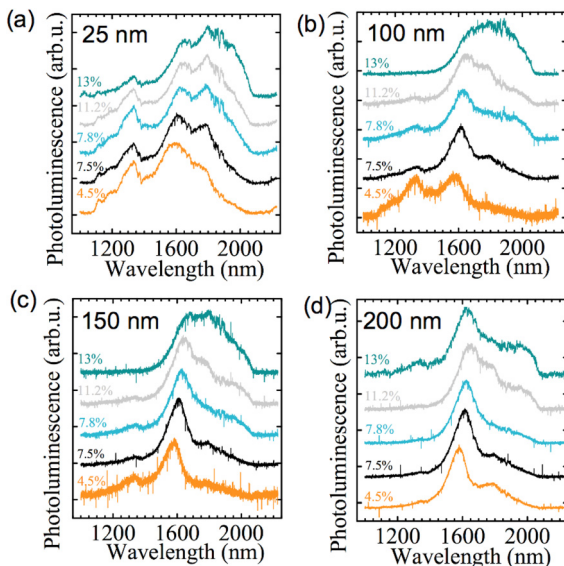


FIG. 3. Room temperature photoluminescence for  $25\text{ nm}$  (a),  $100\text{ nm}$  (b),  $150\text{ nm}$  (c), and  $200\text{ nm}$  (d) thick germanium films grown on InGaAs buffer layers with various indium contents. The effective indium content is indicated on the graphs. The effective indium content accounts for the partial relaxation of the buffer layer. The curves have been normalized and offset for clarity. The luminescence is excited by a He-Ne laser. The small resonance around  $1350\text{ nm}$  is a defect signal from the InGaAs buffer layer.

temperature microphotoluminescence spectra of germanium films with various thicknesses grown on InGaAs buffer layers with various indium contents. The spectra are normalized to the same intensity and offset for clarity. Several features can be directly evidenced. The photoluminescence is generally dominated by the germanium direct band gap recombination that is resonant around  $1600$ – $1650\text{ nm}$ . The indirect band gap recombination is observed around  $1800\text{ nm}$ . Note that there is on some spectra a parasitic atmosphere absorption around  $1800$ – $1900\text{ nm}$  that is more or less pronounced. It gives incorrectly in some cases the impression that several resonances are present on the indirect band gap recombination. As a consequence, it is difficult to precisely assign the position of the maximum resonance for the broad indirect band gap recombination. An additional resonance can be observed on some spectra around  $1350\text{ nm}$ . This recombination band is not associated with germanium but with radiative defects that are present in the InGaAs buffer layers. As expected, this resonance is preferentially observed for the thin  $25\text{ nm}$  layer as the transmission of the germanium layer is larger for this thickness at  $632.8\text{ nm}$ . In most cases, the direct band gap recombination is larger than the indirect band gap recombination. This feature is a direct consequence of the small thickness of the germanium layer that significantly limits the reabsorption of the emission.<sup>23</sup>

For samples with thicknesses up to  $150\text{ nm}$ , there is a clear regular red-shift of the direct band gap recombination as the indium content in the buffer layer is increased. This red-shift is a direct consequence of the increased tensile strain in the germanium layer. In Fig. 4, the resonant wavelength for direct band gap recombination is compared to a modeling of photoluminescence involving heavy holes or light holes recombination based on a 30 band  $\mathbf{k}\cdot\mathbf{p}$  formalism that accounts for strain effect.<sup>8,24</sup> For heavy holes, the spectral shift in energy due to biaxial strain is expected to follow the relation  $\Delta E_{pl} = -7.8 \varepsilon_{||}$  (eV).<sup>25</sup> As seen in Fig. 4, all the data points are clearly consistent with a recombination involving the heavy hole band. This is not surprising as the collection geometry is more favorable for the collection of

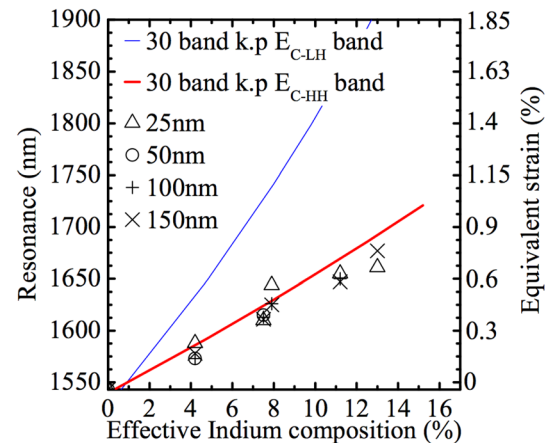


FIG. 4. Comparison between the resonance wavelength of the direct band gap recombination and the one calculated using a 30 band  $\mathbf{k}\cdot\mathbf{p}$  formalism. The calculated resonances of recombination involving heavy holes and light holes are indicated as full lines. The scattered points correspond to the experimental data extracted from Fig. 3.

in-plane polarized light. The amplitude of light hole recombination measured at normal incidence for planar films is expected to be significantly smaller than the one of heavy holes. The peak wavelength shifts following the expected dependence as the indium content increases. An important feature deduced from photoluminescence measurements is that germanium can be coherently strained for thicknesses up to 150 nm and indium buffer layer composition up to 13%, or at least for the spatial region where the luminescence comes from. In the latter case, the recombination maximum occurs at 1677 nm, as compared to 1543 nm for doped germanium on GaAs, corresponding to a biaxial strain of 0.75%. Note that the small compressive strain of Ge on GaAs (0.07%) is taken into account in this derivation. Another interesting feature that can be observed in Fig. 3 is that the ratio between direct band gap and indirect band gap recombination decreases as the indium content of the buffer layer increases. As the strain increases, one would rather expect a more efficient carrier transfer from the  $L$  valley to the zone center  $\Gamma$  valley, hence an increase of this ratio. Meanwhile there is no regular dependence of the amplitude of the photoluminescence as a function of the buffer layer composition. This indicates that non-radiative recombinations are dependent on the indium buffer layer composition. The ratio between direct band gap recombination and indirect band gap recombination depends on several effects: self-absorption for the direct band gap recombination, deviation from quasi-equilibrium conditions due to fast nonradiative recombinations,<sup>26</sup> surface roughness scattering.<sup>27</sup> It is not straightforward to disentangle the role of these different contributions. In the present case, one can suppose that the indirect band gap recombination is enhanced as compared to the direct band gap recombination because of an enhanced scattering for high indium content buffers that provides the momentum needed for indirect recombination. This enhanced scattering might be due to the disorder in the crystal parameters or due to surface roughness scattering.

Figure 5(a) shows the microphotoluminescence spectra for the samples grown on a buffer with an effective indium composition of 11.2%. The spectra have been offset but their

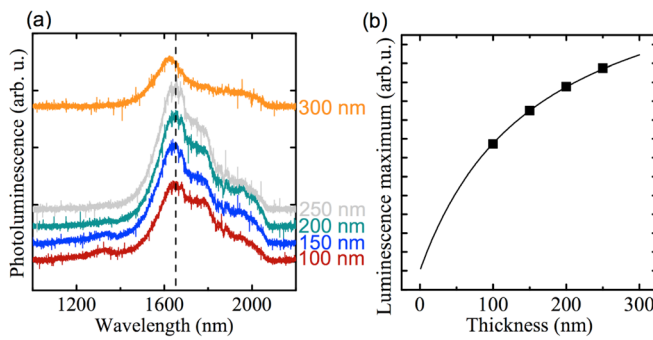


FIG. 5. (a) Room temperature photoluminescence spectra of germanium on  $\text{In}_{0.112}\text{Ga}_{0.888}\text{As}$  for an increasing thickness from 100 to 300 nm. The curves have been offset for clarity. The Ge thicknesses are indicated in the figure. The small resonance at 1330 nm clearly observed on the 100 and 150 nm thick layers are defect signals from the  $\text{InGaAs}$  buffer layer. (b) Photoluminescence amplitude as a function of thickness for 11.2% indium buffer. The experimental data are represented by squares. The full line is a fit accounting for bulk and surface recombination.

amplitude is not normalized. For thicknesses varying between 100 and 250 nm, the resonance wavelength for direct band gap recombination is identical thus indicating that no significant relaxation occurs. The maximum is observed at 1650 nm. This corresponds for heavy hole recombination to a biaxial tensile strain of 0.58%. For the sample with 300 nm thickness, there is a clear blue shift of the resonance peak, indicating that partial relaxation has occurred. The recombination resonance indicates an equivalent biaxial strain around 0.44%. The critical thickness for an 11.2%  $\text{InGaAs}$  buffer layer is thus above 250 nm which is significant. Meanwhile, the amplitude is significantly decreased at 300 nm indicating that this relaxation is associated with an increase of non-radiative recombination. This type of sample is thus not suited to investigate germanium laser emission. It is interesting to follow the dependence of the photoluminescence amplitude as a function of the sample thickness. Two types of non-radiative recombination are considered. The bulk non-radiative recombination associated with either Shockley-Read-Hall or Auger processes ( $\tau_{\text{bulk}}$ ) and the surface recombination characterized by a surface recombination velocity ( $S$ ). The ratio between both types of recombination is dependent on the thickness of the germanium layer. Note that if we take into account the carrier diffusion and considered that all light is absorbed for thicknesses larger than 100 nm, the photo-induced carrier density is estimated to be around  $3 \times 10^{18} \text{ cm}^{-3}$  in these experiments. The germanium sample is  $n$ -doped with a dopant concentration of  $n_0 \sim 10^{19} \text{ cm}^{-3}$ . Auger recombination mechanisms are thus likely to dominate and characterized by a recombination time  $\tau_{\text{Auger}} = 1/C n_0^2$ . Considering an Auger recombination coefficient of  $10^{-30} \text{ cm}^6 \text{ s}^{-1}$ ,<sup>28</sup> the bulk non-radiative recombination is found equal to 10 ns. The photoluminescence of the  $n$ -doped germanium can be estimated under steady state from the hole population  $p$  following:

$$I \propto p \propto \frac{G}{\frac{1}{\tau_{\text{bulk}}} + \frac{2S}{W}}, \quad (1)$$

where  $G$  is the generation term and  $W$  is the thickness of the layer. Figure 5(b) shows the fit of the photoluminescence amplitude according to Eq. (1), leading to a surface recombination velocity of  $800 \text{ cm s}^{-1}$ .

## DISCUSSION

Fig. 6 shows an overview of the results obtained by microphotoluminescence measurements. The strain magnitude is plotted as a function of the layer thickness and as a function of the effective indium content of the buffer layer. The general trend is, for a fixed thickness, an increase of the strain as the indium content increases. This rule is however not obeyed if the indium content or the thicknesses are too large. The shaded area in Fig. 6 highlights the zone observed by photoluminescence where partial relaxation of the germanium film has occurred. This partial relaxation is also associated with a drop in the photoluminescence amplitude. As the challenge to lower the threshold of a germanium laser is to simultaneously increase the strain and the thickness of the

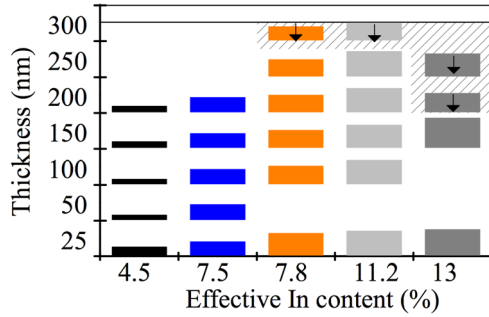


FIG. 6. Biaxial strain magnitude deduced from photoluminescence measurements as a function of germanium thickness and effective indium content. The height of the bars is proportional to the in-plain strain. The shaded area highlights the zone where strong relaxation has occurred. The black arrows indicate a significant decrease in the photoluminescence amplitude.

layer, Fig. 6 shows the trade-off that is necessary to follow in order to keep a high optical quality germanium film. The optimum region, i.e., large strain and high optical quality, corresponds to a germanium thickness around 150–250 nm and an indium content of the buffer layer between 8% and 13%. These values are also compatible with optical waveguiding. If we consider a vertical stacking consisting of GaAs substrate/InGaAs buffer/Ge/air, a minimum thickness of the Ge layer is required if one requires for the optical mode to be significantly confined in the Ge layer. This thickness is approximately of the order of  $\lambda/2n$ , where  $\lambda$  is the mode wavelength to be guided and  $n$  the refractive index of germanium. The variation of refractive index as the function of InGaAs buffer layer composition is weak. The main index change results thus from the index difference between germanium, around 4, InGaAs ( $\sim 3.4$ ) and air (1). Numerical modeling confirms that thicknesses larger than 150 nm are appropriate to confine at  $1.6 \mu\text{m}$  the optical mode in Ge for TE-polarization (electric field parallel to the layer plane). A thickness around 200 nm is necessary at the same wavelength for TM-polarized optical mode. It indicates that lowering the strain magnitude might be more interesting for this polarization. An indium content of the buffer layer less than 11% and a germanium thickness around 200 nm represents the best trade-off for this configuration.

Another striking feature is the quantitative difference in terms of strain magnitude that can be observed between photoluminescence spectra and Raman or X-ray diffraction measurements. Fig. 7 presents a comparison of the biaxial strain amplitude as deduced from X-ray reflection, Raman scattering and room temperature microphotoluminescence. For small thicknesses, there is a good agreement between the different types of measurements. However, a significant deviation is observed for large thicknesses, in a domain where partial relaxation can be observed. This is for example clearly highlighted for the case of the 250 nm thick sample grown on buffer layer with an effective indium content of 13%. The biaxial strain measured by Raman and X-ray reflection is around 0.3% whereas the strain magnitude deduced from photoluminescence is around 0.6%, if we suppose that the energy dependence of the photoluminescence maximum follows the one given by biaxial deformation. Several features might explain the difference. The area probed by X-ray diffraction is

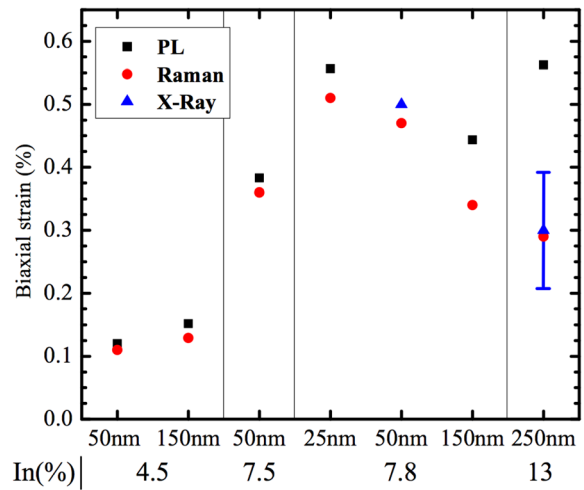


FIG. 7. Comparison of biaxial strain deduced from Raman (dots), microphotoluminescence (squares), and X-ray diffraction measurements (triangles). The horizontal axis shows a combination of indium content of the buffer layer (%) and germanium thickness (nm). The bar for the X-ray measurement of the 13%–250 nm sample highlights the values deduced for two in-plane perpendicular directions (0.39% and 0.21%, average value 0.3%).

large ( $\text{mm}^2$  scale) and significantly larger than the area probed by photoluminescence. The strain value obtained by X-ray is thus an average over a large surface, including the areas where defects and dislocations are present. As the thickness increases, the defect density increases. The microphotoluminescence is highly sensitive to non-radiative recombinations which is not the case for Raman scattering. It is likely that for areas where local defect density is large or in the vicinity of threading dislocations, the radiative efficiency drops because of the enhanced carrier recombination. Defects can also introduce inhomogeneous strain fields that will modify the carrier diffusion and localization.<sup>29</sup> Photoluminescence can only be observed in areas where optically induced carriers are present and the resulting spectra correspond to a local signature of the material properties. Local areas free of defects and with high strain field are more likely to dominate the spectra. It is thus not completely surprising that Raman or X-ray diffraction measurements lead to different results as compared to photoluminescence. Moreover, X-ray diffraction has shown a strong anisotropy in the germanium lattice for samples grown on high indium content buffer layers. This anisotropy is a direct consequence of the material properties of the InGaAs buffer. Different studies have shown that in materials with a strong anisotropic distortion, a large variation of Raman coefficients and phonon deformation potential can be observed.<sup>30</sup> Differences in the absolute values of strain measured by  $\mu$ -photoluminescence,  $\mu$ -Raman, and high-resolution X-ray diffraction have also been observed in nitride materials.<sup>31,32</sup> One can thus expect similar effects to be observed in tensile-strained germanium. While beyond the scope of this article, a detailed study of this anisotropy and inhomogeneous strain field will be the focus of future work. The presence of local defects can be observed by cross-section transmission electron microscopy images. In Ref. 18, we have shown that in the case of a thin germanium sample on InGaAs, a perfect interface is obtained and no specific defects are observed. For the thick and highly-strained sample, cross-sectional transmission

electron microscopy (XTEM) reveals large areas without any threading dislocations. Dislocations are well confined at the interface. We measure an average interdistance of 20 nm at the GaAs/InGaAs interface. This value is very close to the ideal value (22 nm) indicating a total accommodation of the mismatch by interfacial dislocations. The distances between dislocations at the Ge/InGaAs interface along [110] and [1-10] directions are higher than the expected value. It indicates that threading dislocations should be present in the Ge structure. Nevertheless, we never observed these dislocations by XTEM. This indicates a low density. It should be noted that the distance between mismatch interfacial dislocations is not the same along the two ⟨110⟩ in-plane directions. We measure 50 nm and 250 nm respectively. This is in agreement with the anisotropy observed by X-Ray diffraction.

## CONCLUSION

We have studied the optical properties of tensile-strained germanium grown on lattice-mismatched InGaAs buffer layer as a function of both thickness and indium content. Large tensile strain can be transferred into germanium by this approach. The study has evidenced the trade-off between large strain magnitude and film thickness. The critical thickness is for example above 250 nm for samples grown on 11.2% InGaAs buffer layer. Meanwhile, we have observed that the ratio between direct and indirect band gap recombination decreases as the strain field increases. For large thicknesses and large indium content of the buffer layer, X-ray diffraction measurements have shown a strong in-plane anisotropy of the germanium lattice parameters. We have evidenced that in this case, microphotoluminescence and X-ray or Raman measurements provide different values for the in-plane strain. This difference has been attributed to the varying sensitivity of these measurements to the material properties, either local or on spatial average. This work provides a guideline to achieve high optical quality and highly strained germanium films with a thickness compatible with optical waveguiding. This should be useful for the design of a low-threshold germanium laser under optical pumping.

## ACKNOWLEDGMENTS

This work was supported by “Triangle de la Physique” under Gerlas convention and by Agence Nationale de la Recherche under GRAAL convention (ANR Blanc call 2011 BS03 004 01). This work was partly supported by the French RENATECH network.

<sup>1</sup>G. Roelkens, L. Liu, D. Liang, R. Jones, A. Fang, B. Koch, and J. Bowers, *Laser Photon. Rev.* **4**, 751 (2010).

<sup>2</sup>Y. Halioua, T. J. Karle, F. Raineri, P. Monnier, I. Sagnes, G. Roelkens, D. V. Thourhout, and R. Raj, *Appl. Phys. Lett.* **95**, 201119 (2009).

- <sup>3</sup>J. Menendez and J. Kouvetakis, *Appl. Phys. Lett.* **85**, 1175–1177 (2004).
- <sup>4</sup>O. Boyraz and B. Jalali, *Opt. Express* **12**, 5269 (2004).
- <sup>5</sup>L. Tsypbeskov and D. Lockwood, *Proc. IEEE* **97**, 1284 (2009).
- <sup>6</sup>J. Liu, X. Sun, R. Camacho-Aguilera, L. C. Kimerling, and J. Michel, *Opt. Lett.* **35**, 679 (2010).
- <sup>7</sup>J. Liu, X. Sun, D. Pan, X. Wang, L. C. Kimerling, T. L. Koch, and J. Michel, *Opt. Express* **15**, 11272 (2007).
- <sup>8</sup>M. El Kurdi, G. Fishman, S. Sauvage, and P. Boucaud, *J. Appl. Phys.* **107**, 013710 (2010).
- <sup>9</sup>X. Sun, J. Liu, L. C. Kimerling, and J. Michel, *Appl. Phys. Lett.* **95**, 011911 (2009).
- <sup>10</sup>M. El Kurdi, T. Kociniewski, T.-P. Ngo, J. Boulmer, D. Debarre, P. Boucaud, J. F. Damencourt, O. Kermarrec, and D. Bensahel, *Appl. Phys. Lett.* **94**, 191107 (2009).
- <sup>11</sup>Y. Ishikawa, K. Wada, D. D. Cannon, J. Liu, H.-C. Luan, and L. C. Kimerling, *Appl. Phys. Lett.* **82**, 2044 (2003).
- <sup>12</sup>D. Nam, D. Sukhdeo, A. Roy, K. Balram, S.-L. Cheng, K. C.-Y. Huang, Z. Yuan, M. Brongersma, Y. Nishi, D. Miller, and K. Saraswat, *Opt. Express* **19**, 25866 (2011).
- <sup>13</sup>M. de Kersauson, M. El Kurdi, S. David, X. Checouri, G. Fishman, S. Sauvage, R. Jakomin, G. Beaudoin, I. Sagnes, and P. Boucaud, *Opt. Express* **19**, 17925 (2011).
- <sup>14</sup>G. Fishman, *Semi-conducteurs: les bases de la théorie k.p.*, (Physique, Ecole Polytechnique, 2010).
- <sup>15</sup>Y. Bai, K. E. Lee, C. Cheng, M. L. Lee, and E. A. Fitzgerald, *J. Appl. Phys.* **104**, 084518 (2008).
- <sup>16</sup>Y. Huo, H. Lin, R. Chen, M. Makarova, Y. Rong, M. Li, T. I. Kamins, J. Vuckovic, and J. S. Harris, *Appl. Phys. Lett.* **98**, 011111 (2011).
- <sup>17</sup>J. R. Sanchez-Perez, C. Boztug, F. Chen, F. F. Sudradjat, D. M. Paskiewicz, R. Jacobson, M. G. Lagally, and R. Paiella, *Proc. Natl. Acad. Sci. U.S.A.* **108**, 18893 (2011).
- <sup>18</sup>R. Jakomin, M. de Kersauson, M. El Kurdi, L. Largeau, O. Mauguin, G. Beaudoin, S. Sauvage, R. Ossikovski, G. Ndong, M. Chaigneau, I. Sagnes, and P. Boucaud, *Appl. Phys. Lett.* **98**, 091901 (2011).
- <sup>19</sup>F. Cerdeira, C. J. Buchenauer, F. H. Pollak, and M. Cardona, *Phys. Rev. B* **5**, 580 (1972).
- <sup>20</sup>T. S. Perova, J. Wasyluk, K. Lyutovich, E. Kasper, M. Oehme, K. Rode, and A. Waldron, *J. Appl. Phys.* **109**, 033502 (2011).
- <sup>21</sup>F. Pezzoli, E. Bonera, E. Grilli, M. Guzzi, S. Sanguinetti, D. Chrastina, G. Isella, H. von Kanel, E. Wintersberger, J. Stangl, and G. Bauer, *J. Appl. Phys.* **103**, 093521 (2008).
- <sup>22</sup>J. S. Reparaz, A. Bernardi, A. R. Goni, M. I. Alonso, and M. Garriga, *Appl. Phys. Lett.* **92**, 081909 (2008).
- <sup>23</sup>J. R. Haynes, *Phys. Rev.* **98**, 1866 (1955).
- <sup>24</sup>M. El Kurdi, S. Sauvage, G. Fishman, and P. Boucaud, *Phys. Rev. B* **73**, 195327 (2006).
- <sup>25</sup>M. El Kurdi, H. Bertin, E. Martincic, M. de Kersauson, G. Fishman, S. Sauvage, A. Bosseboeuf, and P. Boucaud, *Appl. Phys. Lett.* **96**, 041909 (2010).
- <sup>26</sup>G. Grzybowski, R. Roucka, J. Mathews, L. Jiang, R. T. Beeler, J. Kouvetakis, and J. Menendez, *Phys. Rev. B* **84**, 205307 (2011).
- <sup>27</sup>S.-R. Jan, C.-Y. Chen, C.-H. Lee, S.-T. Chan, K.-L. Peng, C. W. Liu, Y. Yamamoto, and B. Tillack, *Appl. Phys. Lett.* **98**, 141105 (2011).
- <sup>28</sup>R. Conradt and J. Aengenheister, *Solid State Commun.* **10**, 321 (1972).
- <sup>29</sup>W. L. Ng, M. A. Lourenco, R. M. Gwilliam, S. Ledain, G. Shao, and K. P. Homewood, *Nature* **410**, 192 (2001).
- <sup>30</sup>V. Darakchieva, T. Paskova, M. Schubert, H. Arwin, P. P. Paskov, B. Monemar, D. Hommel, M. Heuken, J. Off, F. Scholz, B. A. Haskell, P. T. Fini, J. S. Speck, and S. Nakamura, *Phys. Rev. B* **75**, 195217 (2007).
- <sup>31</sup>U. T. Schwarz, P. J. Schuck, M. D. Mason, R. D. Grober, A. M. Roskowski, S. Einfeldt, and R. F. Davis, *Phys. Rev. B* **67**, 045321 (2003).
- <sup>32</sup>S. Ruvimov, Z. Liliental-Weber, T. Suski, J. W. Ager III, J. Washburn, J. Krueger, C. Kisielowski, E. R. Weber, H. Amano, and I. Akasaki, *Appl. Phys. Lett.* **69**, 990 (1996).